Chandra Observations of the Anomalous X-ray Pulsar 1E 2259+586

Sandeep K. Patel[1], Chryssa Kouveliotou[1,2], Peter M. Woods[1], Allyn F. Tennant[2], Martin C. Weisskopf[2], Mark H. Finger[1], Ersin Göğüş[3], Michiel van der Klis[4], Tomaso Belloni[5]

ABSTRACT

We present X-ray imaging, timing, and phase resolved spectroscopy of the anomalous X-ray pulsar 1E 2259+586 using the *Chandra X-ray Observatory*. The spectrum is well described by a power law plus blackbody model with $\Gamma = 3.6(1)$, $kT_{\rm BB}$= 0.412(6) keV, and $N_{\rm H}$= 0.93(3) $\times$ 10^{22} cm^{-2}; we find no evidence for spectral features (0.5 − 7.0 keV). We derive a new, precise X-ray position for the source and determine its spin period, P = 6.978977(24) s. Time resolved X-ray spectra show no significant variation as a function of pulse phase. We have detected excess emission beyond 4″ from the central source extending to beyond 100″, due to the supernova remnant and possibly dust scattering from the interstellar medium.

Subject headings: pulsars:individual (1E 2259+586) — stars:neutron — X-rays:stars

1. Introduction

X-ray pulsars, typically, have hard spectra and a broad range of observed spin periods (2 ms – 3 hr). There is, however, a group of at least 5 X-ray pulsars (4U 0142+61, 1E 1048.1−5937, 1RXS J170849−40091, 1E 1841−045, 1E 2259+586) that have characteristics similar to one another, but distinct from those known to be accreting binary pulsars.

[1]Universities Space Research Association/NSSTC, SD-50, Huntsville, AL 35805

[2]NASA Marshall Space Flight Center, Huntsville, SD-50, AL 35812

[3]Department of Physics, University of Alabama in Huntsville/NSSTC-SD50, Huntsville, AL 35805

[4]Astronomical Institute "Anton Pannekoek," University of Amsterdam, and Center for High Energy Astrophysics, Kruislaan 403, 1098 SJ Amsterdam, Netherlands

[5]Osservatorio Astronomico di Brera, Via Bianchi 46, 23807 Merate (Lc), Italy

The existence of this class of pulsars, dubbed the 'Anomalous X-ray Pulsars' (AXPs), was first identified as such 6 years ago (Mereghetti & Stella 1995; van Paradijs et al. 1995). AXP characteristics include: (i) predominantly constant X-ray luminosities of order $\sim 10^{35}$ ergs s^{-1}; (ii) relatively soft, two-component X-ray spectra (blackbody $kT_{BB} \sim 0.5$ keV; power-law photon indices $\sim 2.5-4$); (iii) small Galactic scale height ($z_{\rm rms} \sim 56$ pc); (iv) association of 2 out of 5 (1E 1841−045, 1E 2259+586) with young ($\sim 10^{4-5}$ year) supernova remnants (SNRs) (Gaensler et al. 2001); (v) pulse periods within a narrow range (5 – 12 s); (vi) rapid, nearly constant spin-down rates ($10^{-11} - 10^{-13}$ s s^{-1}); and (vii) no clear evidence for a binary companion filling its Roche lobe (see e.g. Mereghetti 1999, for a review).

1E 2259+586 was discovered by Gregory & Fahlman (1980) and lies along the line of sight of an X-ray and radio bright galactic supernova remnant G109.1-1.0 (CTB 109) (Rho & Petre 1997; Hughes et al. 1984). There is no accurate distance measurement for the SNR; Sofue et al. (1983) and Hughes et al. (1984) have estimated distances of 4.1 and 5.6 kpc, respectively, using the surface brightness-diameter relation in different wave bands. The X-ray properties of 1E 2259+586 (and the associated SNR G109.1-1.0) have been investigated using *BeppoSAX*, *ROSAT*, *BBXRT*, and *ASCA* (Parmar et al. 1998; Rho & Petre 1997; Corbet et al. 1995). The pulsar spectrum has often been described as an absorbed powerlaw (PL) with a photon spectral index of $\Gamma = 4.0$ and a blackbody (BB) component with a characteristic temperature of $kT_{\rm BB}$= 0.43 keV with galactic absorption column density of $N_{\rm H}$=0.9×10^{22} cm^{-2} (Rho & Petre 1997).

The best previous position for 1E 2259+586 was $\alpha = 23^{\rm h}\ 01^{\rm m}\ 08^{s}.44$, $\delta = 58^{\circ}\ 52'\ 44''.1$ (J2000) with a 95% confidence error radius of $2''.2$ established by Hulleman et al. (2000) using *ROSAT* HRI observations. They found no optical counterpart with the Keck, down to limiting magnitudes of $R = 25.7$ and $I = 24.3$. Coe et al. (1994) set an upper limit with the VLA to the 1.5 GHz flux of 50 μJy.

We present here an analysis of our *Chandra* observation of the source. In §2 we describe the observations and present imaging, timing and spectral results. The analysis and derivation of a new precise position of $\alpha = 23^{h}\ 01^{m}\ 08^{s}.295$, $\delta = +58^{\circ}\ 52'\ 44''.45$ (J2000) with a 99% confidence error radius of $0''.60$, together with the K-band identification of 1E 2259+586 is discussed in the companion paper by Hulleman et al. (2001).

2. Observations and Results

1E 2259+586 was observed on 11 January 2000 using the Advanced CCD Imaging Spectrometer (ACIS). Data were collected sequentially in two different observing modes:

timed exposure (TE) mode (19 ks) and continuous clocking (CC) mode (12 ks). Data obtained in TE mode allow for two-dimensional imaging. Accurate spectroscopy of the bright pulsating target is limited due to pulse pile up. Pulse-phased spectroscopy is further limited by the 3.24 s time resolution. In CC mode the amount of pileup is negligible due to its 2.85 ms time resolution, allowing for both accurate time integrated and phase-resolved spectroscopy. Furthermore, one can exploit the one-dimensional image to search for extension of the central source.

The source was positioned on the nominal target position of ACIS-S3, a back illuminated CCD on the spectroscopic array (ACIS-S) with good charge transfer efficiency and spectral resolution (Townsley et al. 2000). In addition to S3, four front illuminated CCDs were active (I2, I3, S2 and S4, see also Figure 1). The focal plane operating temperature was -110° C.

Standard processing of the data was performed by the *Chandra* X-ray Center. The data were filtered to exclude events with *ASCA* grades 1, 5, and 7, hot pixels, bad columns, and events on CCD node boundaries. We removed the serial clocking noise streaks from S4 using the *destreak* program. We examined the processed data and found no times with bad aspect. The S3 light curve was inspected in a region offset from the AXP to identify periods of high background rates: we removed segments where the background exceeded a 3σ threshold about the mean. The resulting useful observing times are 15600 s and 9000 s for TE and CC mode data, respectively.

2.1. Extended Emission Search

Searching for extended emission in the vicinity of 1E 2259+586 was difficult. One must account for numerous contributions to the observed flux. These contributions include not only the bright source itself and the instrumental background, but also the SNR, stars in the field, and diffuse emission from the galactic plane. One must also account for the possibility of a dust scattering halo and/or an X-ray nebula.

To avoid issues related to the effects of pileup in the TE mode data, we first utilized the one dimensional image from the CC mode. We generated a time-integrated image ($0.5 - 7.0$ keV) minus any point sources other than 1E 2259+586. We then subtracted an average count rate intended to remove instrumental and cosmic diffuse X-ray background, as measured by S3 (Markevitch & Vikhlinin 2001, and references therein). Next, we constructed what will be referred to as the "pulsed" image. We took the observed pulse profile, normalized it to a mean of zero and convolved it with the event list of S3. Each count recorded on S3 was assigned a phase. Events with a phase near pulse maximum, regardless of their position

on the chip, received a positive weight and likewise, those near pulse minimum, a negative weight. In doing so, we remove all emission components in our image that do not vary in phase (i.e., everything except the central pulsar). Note that the time delay for photons scattered by the interstellar dust is on average minutes, much longer than the pulsar period.

To improve statistics, we folded the one-dimensional images about the common centroid and accumulated "quasi-radial" profiles. The time-integrated (CC_t) and pulsed (CC_p) profiles are shown in Figure 2. We find that the pulsed radial profile is consistent with the MARX (Wise et al. 1997, v3.01) derived point spread function (PSF).

Next, we collapsed the TE mode observation to mimic the 1-D CC image (Figure 2, TE). We find that the TE profile completely overlaps the CC_t profile beyond $\sim 4''$, marking the radius beyond which the effects of pile-up are negligible. In both profiles we find excess emission beyond $\sim 4''$ which is likely due to the combination of the underlying SNR, a dust-scattering halo and potentially an X-ray plerion. We conclude that the majority of the 1E 2259+586 X-ray flux is contained within a radius of $\sim 4''$. Inspection of the spectra extracted from S3 in five annuli, centered on the pulsar position, and with inner and outer radii of $4'' - 20''$, indicates the presence of continuum radiation in the vicinity of the pulsar. Detailed modeling of the angular and spectral distribution is underway for an accurate accounting of the light, to establish the relative contributions from the SNR, dust scattered light from the pulsar, and any possible plerionic emission. This work will be presented elsewhere.

2.2. Timing Results

High resolution timing with ACIS is only possible using CC-mode data. The CC mode event times denote when the event was read out of the frame store, not when it was detected. We corrected for this effect by assuming that all photons were originally detected at the nominal target position. We removed the variable time delay due to spacecraft dither and telescope flexure using the ACIS CC mode absolute time corrector[6]. The event arrival times were then corrected to the solar system barycenter using *axbary* which utilizes the JPL planetary ephemeris DE-200.

The data were divided into ten $\sim$ 1200 s intervals and individual pulse profiles were derived using epoch folding. These ten profiles were compared to the pulse profile using all the data and the relative phases were fit with a linear function. The resulting pulse period

[6]http://wwwastro.msfc.nasa.gov/xray/ACIS/cctime/

of 6.978977(24) s is referred to epoch MJD 51555.0. This period is consistent with the spin history of the source (Gavriil & Kaspi 2001). The pulse profile is shown in Figure 3a; the 0.5−7.0 keV background subtracted peak-to-peak pulse fraction, as defined in Ozel et al. (2001), is $35.8 \pm 1.4\%$.

Previously, Mereghetti et al. (1998) have established limits as to the existence of a binary companion. They concluded that a putative companion must be a white dwarf or a He-burning star with $M \lesssim 0.8 M_{\odot}$ (for a companion star filling its Roche lobe). We have also searched for evidence of binarity. Binning the data in 50 s intervals, a total of 177 pulse profiles were cross-correlated to the average pulse profile, and pulse phase offsets were determined. We then searched for the sinusoidal signature of a circular binary orbit, for periods ranging from 100 to 5×10^4 s using the method described by Wilson et al. (1999). We found no evidence for binarity and set a 99% confidence limit of $a_x \sin i < 70$ lt-ms for orbital periods in the range from 170 to 5000 s (see also Mereghetti et al. 1998).

2.3. Spectral Analysis

2.3.1. Phase Averaged Spectroscopy

We use CC mode data to obtain an X-ray spectrum. We assume that the CC and TE spectral responses are identical. To test this assumption, we compared low count rate data from a particular region in both CC and TE mode and found reasonable agreement. We define the source by selecting an interval ±8 pixels ($\pm \sim 4''$) (see also §2.1) around the peak flux along the collapsed CC mode axis. The background was determined using two adjacent segments 12 pixels wide for a total area 1.5 times the source area; the background flux provides $\sim 2\%$ of the total flux in the source region. Source and background spectra and response files were generated using the CIAO (v2.1.1) tools *dmextract*, *mkrmf*, and *mkarf*. The extraction was performed in pulse invariant (PI) space (*i.e.*, after the instrument gains were applied). The spectrum was grouped into bins that contained at least 25 events.

All spectral fits were limited to the $0.5 - 7.0$ keV band and use XSPECv11.01 (Arnaud 1996), the photo-electric absorption coefficients of Bałucińska-Church & McCammon (1992), and abundances of Anders & Grevesse (1989). We fit the data to a PL+BB model ($\chi^2/d.o.f. = 316.1/272$); the fit is significantly improved ($\chi^2/d.o.f. = 262.5/258$) by ignoring the 1.9-2.1 keV band, which contains the iridium-edge structure in the telescope response. The best fit PL+BB parameters are $\Gamma = 3.6 \pm 0.1$, $kT_{\rm BB} = 0.412 \pm 0.006$ keV, and $N_{\rm H} = 0.93 \pm 0.03 \times 10^{22}$ cm^{-2}, consistent with the same model results of Rho & Petre (1997). Assuming a source distance of 4 kpc, the 2-10 keV unabsorbed flux and X-ray lumi-

nosity are $2.0 \pm 0.2 \times 10^{-11}$ ergs s^{-1} cm^{-2} and $3.8 \pm 0.4 \times 10^{34}$ ergs s^{-1} respectively. The PL component contributes 50% of the total 2-10 keV unabsorbed flux. Figure 4 shows the data, the best-fit model, and the residuals. We have also investigated single component PL, BB, and bremsstrahlung (BS) models and a combined PL+BS model and found that they are all statistically unacceptable at $> 99.9, > 99.9, > 99.7$, and $> 96.4\%$ confidence levels, respectively.

We have searched for spectral lines. Features that appear below ~ 1 keV and in the Ir edge, are likely due to uncertainty in the spectral response. To set upper limits, we examined two small deviations at 0.7 and 5.0 keV. The addition of a line, modeled by a Gaussian with an intrinsic width of 40 eV at 5.0 keV to the PL+BB model, results in an F statistic of 3.3; the 90% confidence upper limit on the line flux is 8.6×10^{-13} ergs cm^{-2} s^{-1}. Similarly, including a "line" at 0.7 keV gives an F statistic of 1.3. We conclude that there are no significant line features.

2.3.2. Phase Resolved Spectroscopy

We fit the data from each of the ten pulse phase bins (Figure 3) with a PL+BB model parameters free to obtain their best fit values and with $N_{\rm H}$ constrained to be identical at each phase. The fitting gave a column density of $0.93 \pm 0.04 \times 10^{22}$ cm^{-2} (and is identical to the time averaged value found in §2.3.1). For the remaining fits, $N_{\rm H}$ is constrained to be identical at each phase (i.e., linked). We next fit all phase bins with $kT_{\rm BB}$ constrained to be identical at each phase and allow Γ and the normalizations to vary. The decrease in χ^2 was not significant indicating the fits were statistically equivalent. However, there were significant variations in Γ (± 0.2). The fits were repeated with Γ constrained with respect to phase and with $kT_{\rm BB}$ and normalizations allowed to vary. Again this resulted in a statistically equivalent fit but with significant variations of $kT_{\rm BB}$ (± 0.02 keV). The evolution of spectral parameters is shown as a function of pulse phase in Figures 3b and 3c. We fit the spectra with $kT_{\rm BB}$ and Γ constrained to be identical at each phase with only the normalizations free to vary with phase and find that the fits are not statistically equivalent. These results indicate that there is marginal ($\sim 3\sigma$) evidence for evolution in either Γ, $kT_{\rm BB}$ or some combination thereof with phase, but we are unable to determine which. Finally, we impose an additional constraint where the ratio of the PL and BB model normalizations ($\rm PL_{Norm}$, $\rm BB_{\mathit{Norm}}$) are constant. Our fits show no statistical improvement in complicating the model by allowing the normalizations to be independent. Fit statistics for the models discussed are given in Table 1.

3. Discussion

We have observed the anomalous X-ray pulsar, 1E 2259+586 with *Chandra* and determined a new, precise position of the source of $\alpha = 23^h\ 01^m\ 8^s.295$, $\delta = +58^\circ\ 52'\ 44''.45$ (J2000) with a 99% confidence error radius of $0''.60$. We report in the accompanying paper (Hulleman et al. 2001) the details of the derivation, which led to the identification of a near infrared (NIR) counterpart at the *Chandra* position. This is the second AXP counterpart to be found in NIR wavelengths (Hulleman et al. 2000).

We find that of the spectral models we have considered, the PL+BB one is statistically preferred for the pulsar spectrum. In addition, the superb *Chandra* spatial resolution allows us to determine that there is emission extending up to $100''$ from the pulsar, but we are unable to determine its precise origin - whether from the supernova remnant, and/or a dust scattering halo, and/or a plerion.

We acknowledge support from the following grants: MX-0101 (C.K.), NAG5-9350 (P.W.), GO0-1018X (S.P.). We thank F. Paerels and J. Vink for many useful discussions.

REFERENCES

Anders, E. & Grevesse, N. 1989, Geochim. Cosmochim. Acta, 53, 197

Arnaud, K. 1996, in ASP Conf. Ser. 101: Astronomical Data Analysis Software and Systems V, G. H. Jacoby & J. Barnes (eds), 5, 17

Bałucińska-Church, M. & McCammon, D. 1992, ApJ, 400, 699

Coe, M. J., Jones, L. R., & Letho, H. 1994, MNRAS, 270, 178

Corbet, R. H. D., Smale, A. P., Ozaki, M., Koyama, K., & Iwasawa, K. 1995, ApJ, 443, 786

Gaensler, B. M., Slane, P. O., Gotthelf, E. V., & Vasisht, G. 2001, ApJ, 599, 963

Gavriil, F. P. & Kaspi, V. M. 2001, in Submitted to ApJ, astro-ph/0107422

Hughes, V. A., Harten, R. H., Costain, C. H., Nelson, L. A., & Viner, M. R. 1984, ApJ, 283, 147

Hulleman, F., van Kerkwijk, M. H., & Kulkarni, S. R. 2001, ApJ, this volume

Hulleman, F., van Kerkwijk, M. H., Verbunt, F. W. M., & Kulkarni, S. R. 2000, A&A, 358, 605

Markevitch, M. & Vikhlinin, A. 2001, in Submitted to ApJ, astro-ph/010593

Mereghetti, S. 1999, in *The NS-BH Connection*, astro–ph/9912207

Mereghetti, S., Israel, G. L., & Stella, L. 1998, MNRAS, 296, 689

Mereghetti, S. & Stella, L. 1995, ApJ, 442, L17

Ozel, F., Psaltis, D., & Kaspi, V. M. 2001, ApJ in press, astro-ph/0105372

Parmar, A. N., Oosterbroek, T., Favata, F., Pightling, S., Coe, M. J., Mereghetti, S., & Israel, G. L. 1998, A&A, 330, 175

Rho, J. & Petre, R. 1997, ApJ, 484, 828

Sofue, Y., Takahara, F., & Hirabayashi, H. 1983, PASJ, 35, 447

Townsley, L. K., Broos, P. S., & Nousek, J. A. 2000, in preparation

van Paradijs, J., Taam, R. E., & van den Heuvel, E. P. J. 1995, A&A, 299, L41

Weisskopf, M. C. et al. 2000, ApJ, 536, L81

Wilson, C. A., Dieters, S., Finger, M. H., Scott, D. M., & van Paradijs, J. 1999, ApJ, 513, 464

Wise, M. W., Huenemoerder, D. P., & Davis, J. E. 1997, in ASP Conf. Ser. 125: Astronomical Data Analysis Software and Systems VI, Vol. 6, 477

Table 1. Phase Resolved Spectral Fit Results for 1E 2259+586

	Model Settings[a]			
$\mathrm{PL_{Norm}} \propto \mathrm{BB}_{Norm}$	kT_{BB} Linked	Γ Linked	χ^2/ν	$F-$Statistic[b]
Y	Y	Y	1088.4/1050	...
N	Y	Y	1072.7/1040	1.53 (1.84,2.34)
N	Y	N	1049.1/1031	2.04 (1.60,1.92)
N	N	Y	1051.1/1031	1.92 (1.60,1.92)
N	N	N	1042.9/1022	1.59 (1.49,1.74)

[a]Model normalizations for each phase bin are free (unconstrained) to obtain its best fit value while N_{H} is linked (constrained to be identical at each phase) for all model variations.

[b]The numbers in parenthesis correspond to the $F-$statistic needed to claim that the given model is significantly better at the 95% and 99% confidence levels, respectively.

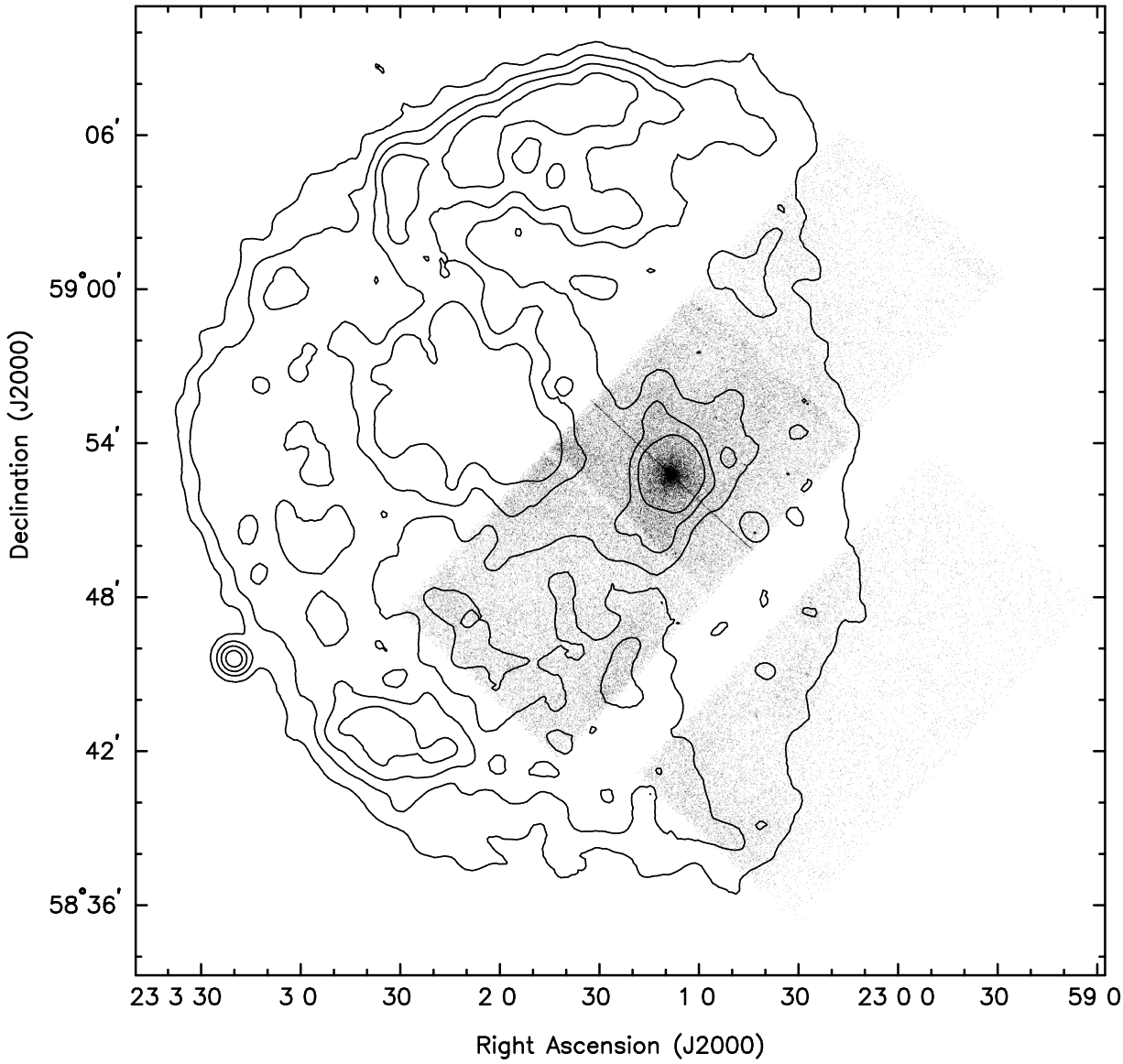

Fig. 1.— *Chandra* ACIS $0.5 - 7.0$ keV image processed as described in § 2.3. The bright line that passes throught the source is the ACIS transfer (or trailed) image (Weisskopf et al. 2000). The false grey scale represents the number of counts detected. The *ROSAT* image (Rho & Petre 1997) is superimposed for comparison and to give a better view of the SNR.

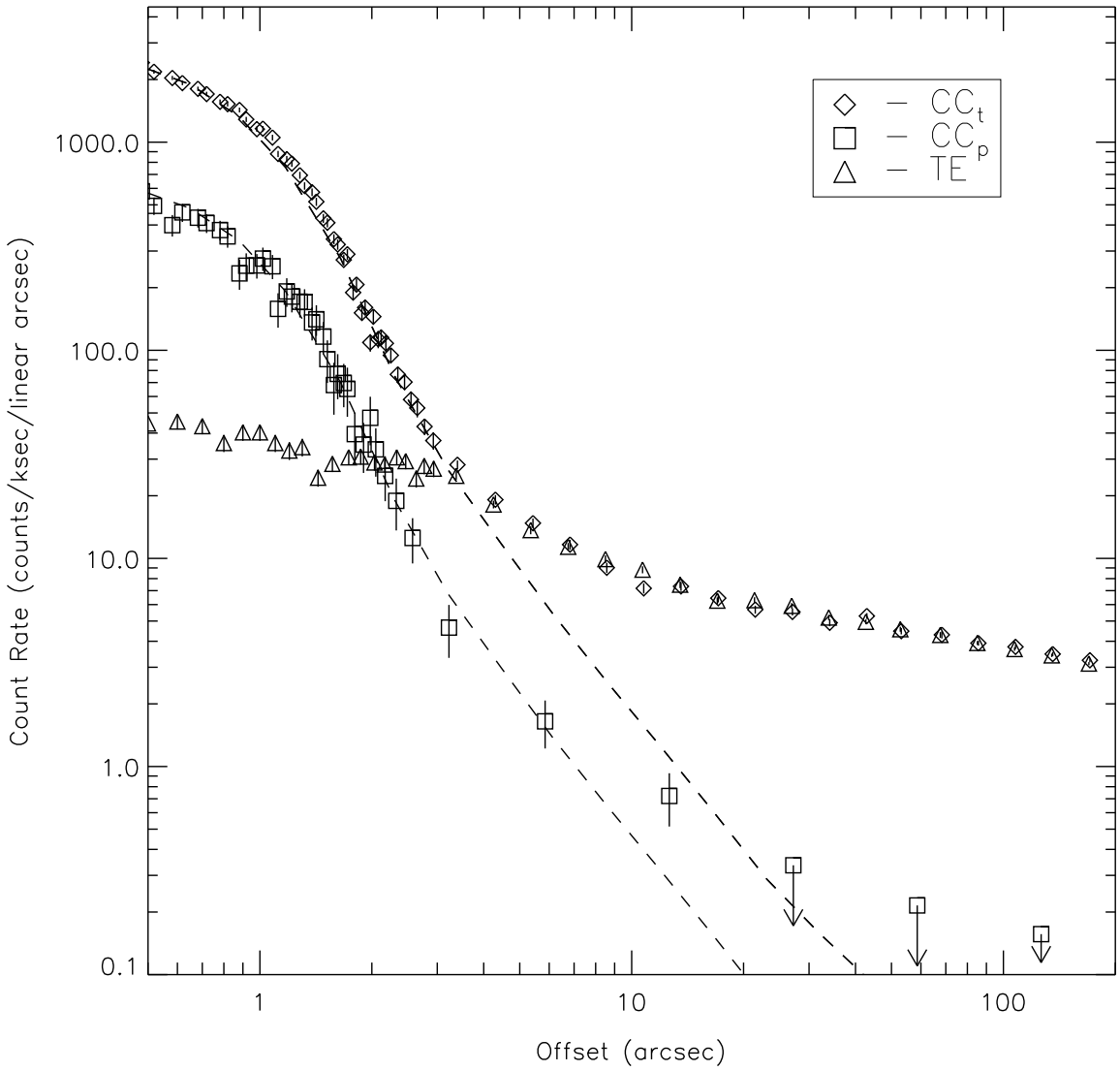

Fig. 2.— Radial surface brightness profiles of the total (CC_t) and pulsed (CC_p) emission (0.5−7.0 keV). The dashed lines are the simulated *Chandra* point spread function. Downward pointing arrows denote 2σ upper limits to the count rate. The triangles are TE mode data. Note the agreement between the total CC profile and the TE profile at radii $\gtrsim 4''$.

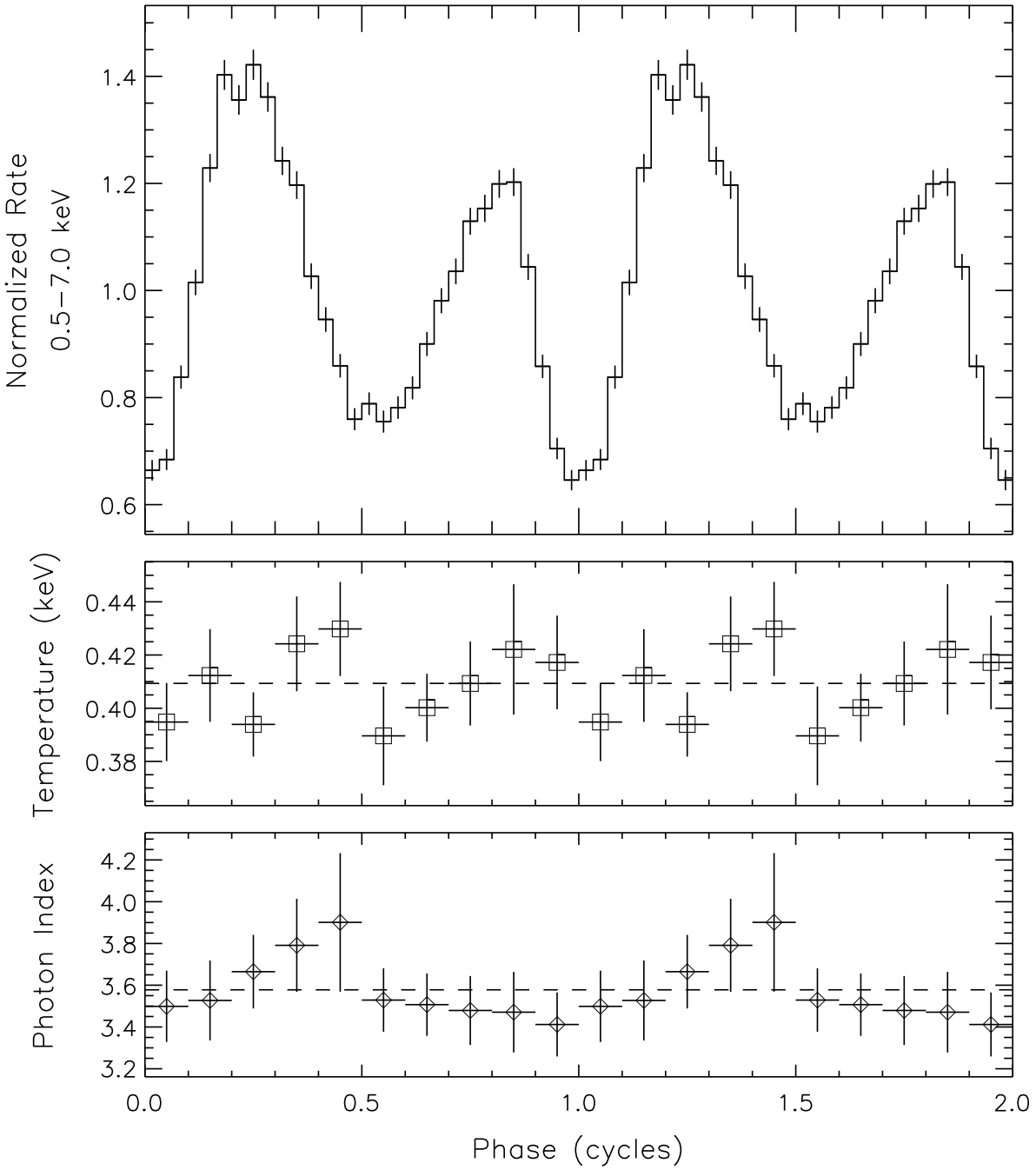

Fig. 3.— Top panel (a): The pulse profile ($0.5 - 7.0$ keV). Middle panel (b): Variation of the blackbody temperature from fitting each phase bin with a PL+BB model. The time averaged value is denoted by the dashed line. Bottom panel(c) : Variation of the PL index. All errors shown denote 1σ.

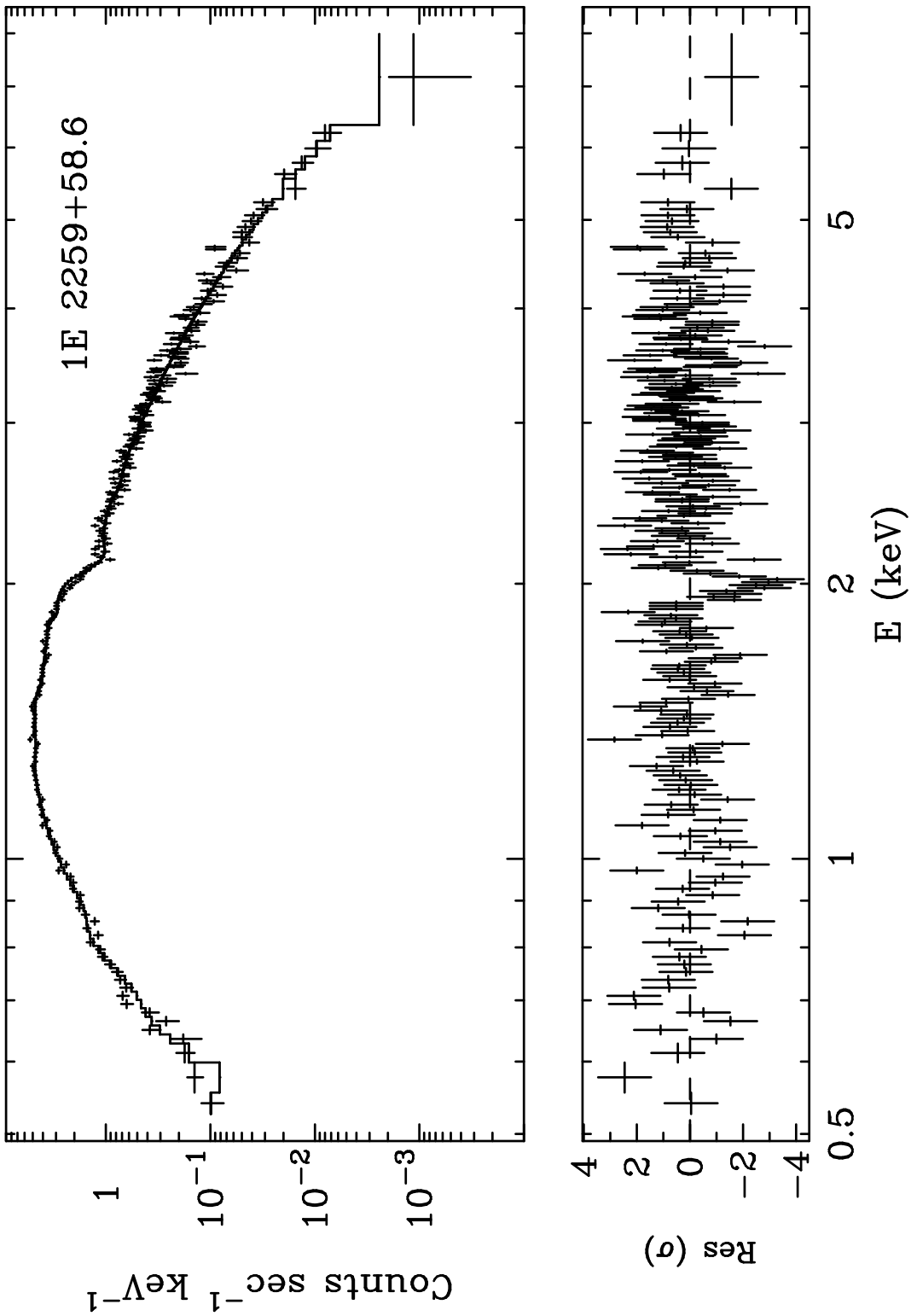

Fig. 4.— The best fit spectral model (PL+BB) and residuals in units of σ. The feature at $\sim$ 2.0 keV appears to be due to a small shift of the location of the Ir absorption edge between the response and the data.